JOURNAL OF KUFA–PHYSICS
www.uokufa.edu.iq/journals/index.php/jkp | ISSN: 2077–5830

A Electron transport study on ultrathin armchair graphene nanoribbone

Aqeel Mohsin Ali

Department of material science, Polymer Research Center، University of Basrah, Basrah-Iraq .

Corresponding Author E-mail: aqeel.mohsin@uobasrah.edu.iq

ARTICLE INF.:

Article history:
Received: 17 JUN, 2019
Accepted: 29 AUG, 2019
Available Online: 25 DEC, 2019

Keywords:

Electron transport
ultrathin armchair graphene nanoribbone
tight-binding approximation

ABSTRACT

Using first-principles quantum transport simulations, this work examines changes in the total electronic currents within the plane of short ultrathin graphene nanoribbon with armchair edges (AGNR). A 5-AGNR-M (M = 4,12,20 and 28 zigzag line) junction was simulated and its transmission were analyzed. The I-V curves under external bias exhibit remarkable semiconducting characteristics. It further demonstrates that the length of the junction also showed significant effects in the determination of the semiconducting nature. More importantly, a significant increasing by double in bias voltage threshold of I–V characteristics have been observed for the positively charged nanoribbon in the family of 5-AGNRs.

DOI: http://dx.doi.org/10.31257/2018/JKP/2019/110209

دراسة أنتقال ألالكترونات خلال شريط نانوي ضيق من الكرافين

عقيل محسن علي

قسم علوم المواد –مركز أبحاث البوليمر-جامعة البصرة

الكلمات المفتاحية:

أنتقال الالكترونات
شريط نانوي كرافيني
تقريب الربط القوي

الـــخُـــلاصـــة

بأستخدام محاكاة الانتقال الكمي بألاعتماد على طريقة المبادئ الاولية أجريت دراسة التيار الالكتروني في مستوي شريط نانوي من الكرافين من نوع حافة الكرسي وبخمس خطوط عرضية. كانت الوصلة تحت الدراسة بأطوال مختلفة وتم تحليل دالة الانتقال. تمت ملاحظة أن منحنيات الجهد ـ التيار تتصرف تبعا لمميزة أشباه الموصلات وتتأثر كثيرا بطول الوصلة. ومن النتائج المهمة في هذه الدراسة هو ملاحظة أن جهد العتبة يتضاعف عندما يكون شريط الكرافين النانوي مشحونا بالشحنة الموجبة.

1. INTRODUCTION

The Graphene nanoribbons (GNRs) are quasi-one-dimensional structures induced by quantum confinement along one in-plane direction [1,2]. The electronic and magnetic properties of GNRs have strongly dependence on the ribbon width and the geometry along the boundary [3-7]. The nanoribbon has the finite band gap induced by the quantum

confinement effect depending on its width of the transport channel, and band gaps suitable for room temperature applications are reached for widths in the low nanometer regime [1,8,9]. On the other hand, the shortest ultrathin-ribbons have promising applications in next-generation Nano-electronic and optoelectronic devices. Many experimental approaches shown controlling the width and edge structures of ultrathin-GNRs. Recent experiments have reported a surface based protocols to prepare atomically precise N=5, 6, 7, 8, 9, 10, 13, 15, 18 and 21 AGNRs from small molecular precursors on Au(111) or Ag(111) single crystals [10-24]. Many theoretical studies have been devoted into investigating the electronic properties of AGNRs, such as density functional theory (DFT) calculations, tight binding calculations, and many-electron green's function approach [25,26]. Most of the theoretical investigations have been carried out with DFT calculations, and other methods such as tight-binding calculations have been adapted to correct DFT calculations. Kimouche *et al.* described the synthesis of the 5-AGNR on the Au(111) substrate using the on-surface polymerization with dibromoperylene $C_{20}H_{10}Br_2$ (DBP) as the molecular precursor [27]. They characterized two ribbon lengths (12 and 20 zigzag lines) to highlight how the ribbon electronic states change with length. Their results demonstrated in ultrathin AGNR's with short lengths of 4 nm reach near-metallic regime with ~200 meV. In addition, they confirm these theoretical predictions in long AGNRs that should exhibit metallic behavior with ~100 meV band gap. Based on Kimouche's experimental results, Zhang *et al.* have evaluated the effect of pentagonal contacts on the transport properties of shorter 5-AGNRs by non-equilibrium Green's functions combined density functional theory [28]. They show that, the conductance and the current can be tuned to be either smaller or larger than that of the perfect AGNR.

The aim of this work is to make further understand for the electronic properties and transport properties of 5-AGNRs. The band structure and transmission is typically investigated by density functional tight binding (DFTB). The narrowest ribbons were selected based on the experimental study of Kimouche [27].

2. COMPUTATIONAL METHOD

Fig.1

Computations of geometrical optimizations, band structures and electron transport are performed by using the DFTB module implemented in Materials Studio software suite 7.0 (Accelrys Inc.). Periodic boundary conditions are used and the inter-graphene distance was kept to a minimum of 50 Å to avoid lateral interactions. The armchair edges are fully passivated with hydrogen atoms. The Fig 1. shows the unit cell of ultrathin AGNR that used in this work. The geometry optimization was performed by using self-consistent-charge tight-binding (SCC-DFTB). The Slater–Koster parameter file mio was employed in SCC-DFTB part of the calculations. The structures of the GNRs studied here are fully relaxed according to the forces and stress on the atoms using the conjugate gradient minimization until the maximum force tolerance being less than 0.02 eV/Å. Finite temperature Fermi smearing is used to control electron state population near to the Fermi level with temperature kT=0.001 Ha. The self-consistent calculations are performed with a charge mixing amplitude of 0.2, and the SCC tolerance is taken as 1×10^{-5}.

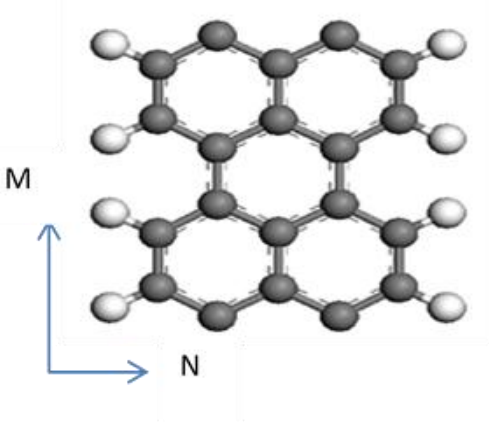

Fig 1: A ball-stick model for an 5-AGNR which has N=5 C-C dimer lines making up its width, and has M zigzag lines forming up its length.

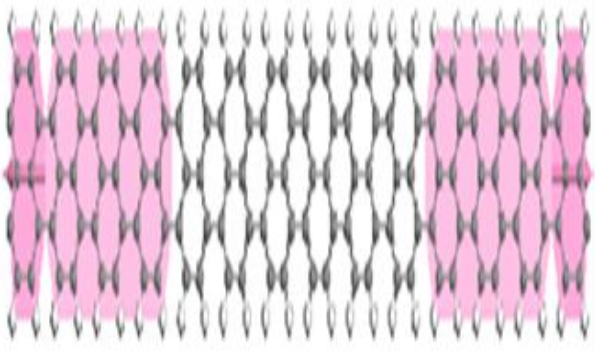

Fig 2: The 5-AGNRs device structure in this study.

To perform reliable simulations, the transport calculations are carried out within the framework of density functional theory based SCC-DFTB combined with nonequilibrium Green's function (NEGF) method. In addition, when referring to the length of a 5-AGNR here, we define the central channel region of the device has the width N=5 (the number of carbon atoms along the transverse direction) and channel length M= 4, 12, 20 and 28 (the number of zigzag lines within the channel region), and the graphene nanoribbons are denoted as M4, M12, M20 and M28. The central channel region is sandwiched in between the left (source) and the right (drain) AGNR electrodes with the same width as the channel and the semi-infinite length.

A two-probe system made of two principal layers each one (~15.8 Å in length), a schematic device is shown in Fig 2. The SCC-DFTB Hamiltonian is used to calculate the transmission coefficients T(E, V), and the current-voltage characteristics were calculated using Landauer-Buttiker formalism. A k point separation of 0.02 yield a good balance between computational time and accuracy in the results.

3. RESULTS AND DISCUSSION

3.1 Band structure

First-principles calculations show that the infinite 5-AGNR possess a non-zero, direct band gaps at the Γ point. This gap arises from both quantum confinement and the crucial effect of the edges, as shown in Fig 3. The highest valance and lowest conduction bands originate from π- and π∗-states, respectively. Unlike the perfect 2D graphene, where π- and π∗ -bands cross at the K-corners of Brilluion zone, infinite 5-AGNR is a direct band gap material having band gap of small value E_g=103 meV. This value is agreed with the theoretical predictions and experimental measuring of Kimouche *et al.*, where they confirms the actual HOMO–LUMO gap extrapolates to value of 100 meV in long 5-AGNRs (≥5nm in length). The armchair nanoribbon is therefore semiconducting, and shows partly-flat electronic band

structures near the Fermi energy, and the corresponding wavefunction is localized. The highest subband can be fitted by a parabola, and obtain an electron effective mass of $m^*_e = 0.18\ m_e$. The hole effective mass is $m^*_h = 0.49\ m_e$. From the linear slope it can to extract the electron velocity $v = 0.39 \times 10^6$ m/s (the hole velocity is 0.15×10^6 m/s), which is smaller than the experimental value (3×10^6 m/s) [29-31].

It is interesting to further note that for the 5-GNRs-M, the band gap decreases as the ribbon length increases, where these values are in good agreement with Kimouche experimental gaps for M12, $M20^+$ and M∞, see table 1.

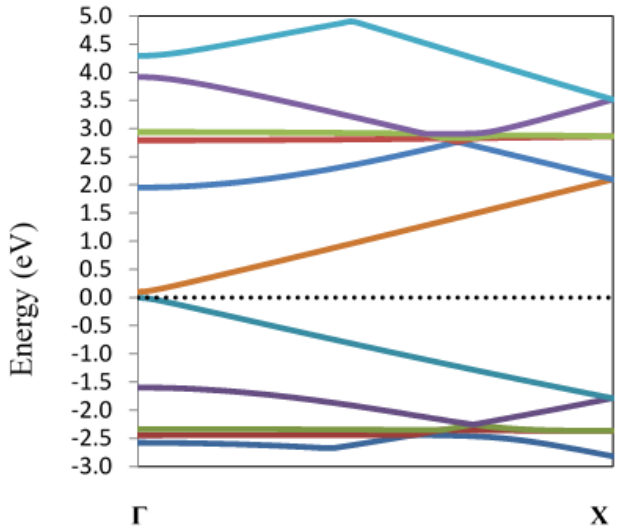

Figure 3: Calculated band structure of infinite 5-AGNRs. The band structures are plotted along the high symmetry path: Γ (0, 0, 0) → X (0.5, 0, 0). The Fermi level (dotted line) is shifted to 0 eV.

The predicted band gaps have strong dependence on the strip length. An interesting point to notice is the fact that model calculations predict that the band gap of M20 is narrowed upon charging. As discussed in Kimoche paper, the charges transfer from the studied 5-AGNR-20 to Au(111) substrate, indicating the presence of oxidation of ribbon M20 and reduction of substrate. The doping of graphene by metallic contacts can be described by charge transfer between the metal and graphene due to differences in work functions.

Table 1: Band gap at Γ point in compared with experimental values [27].

Property	E_{gcal} (eV)	E_{gexp} (eV)
M4	2.03	--------
M12	0.75	0.70
M20	0.48	---------
M20+	0.20	0.20
M28	0.21	---------
M∞	0.10	0.10

In order to create a semiconductor with a desirable band gap the nanoribbon length should be adjusted accordingly. This property of adjusting the band gap makes graphene an excellent candidate for transistor switching. To provide for an intuitive understanding of the transport phenomena, the band structure of the scattering region in their primitive unit cell is shown in Fig 1. A direct band gap improves the carrier mobility because no phonon emission or annihilation is required to satisfy momentum conservation during the electronic transition. As plotted in Figs 4, 5 and

6, the valence and conduction band edges exhibit flat features along the Γ-X direction with very small dispersion in first Brillouin zone. The flat bands actually have small dispersions due to the direct hopping of electrons between adjacent edge atoms along the edges of the AGNRs. Therefore, the conductivity of considered systems in the armchair direction is low in this direction.

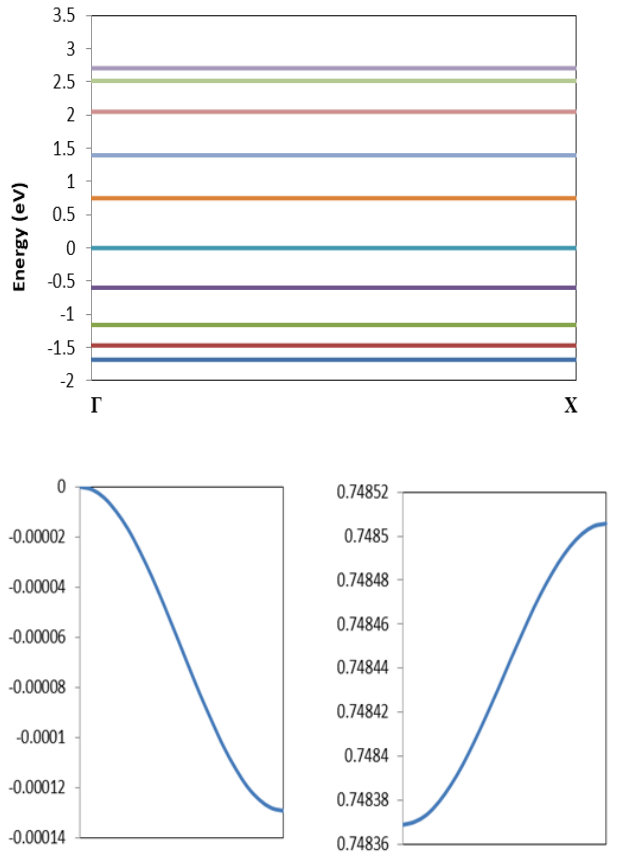

Figure 4: a) Calculated band structure of 5-AGNRs-12. b) Valance band. c) Conduction band. The band structures are plotted along the high symmetry path: Γ (0, 0, 0) → X (0.5, 0, 0). The Fermi level is shifted to 0 eV.

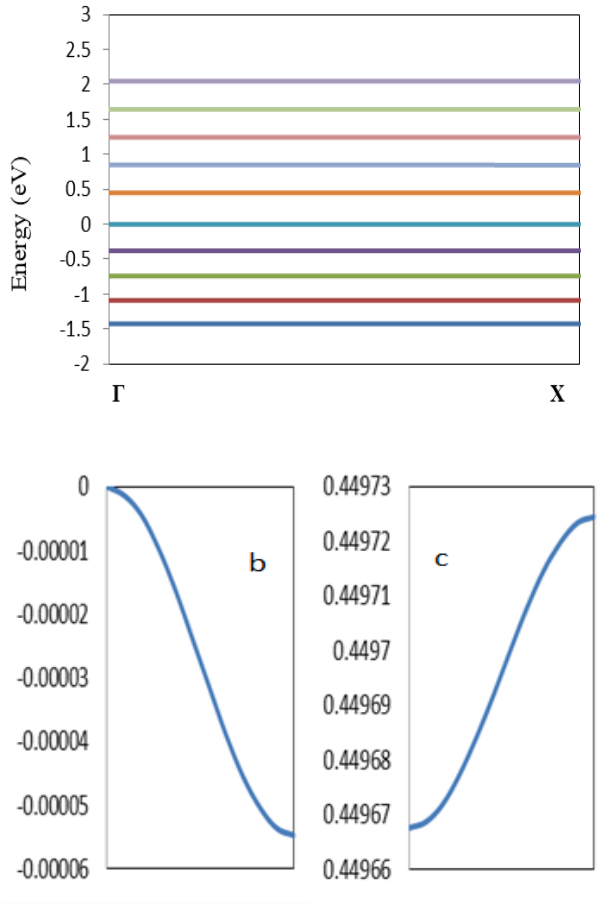

Figure 5: a) Calculated band structure of 5-AGNRs-20. b) Valance band. c) Conduction band. The band structures are plotted along the high symmetry path: Γ (0, 0, 0) → X (0.5, 0, 0). The Fermi level is shifted to 0 eV.

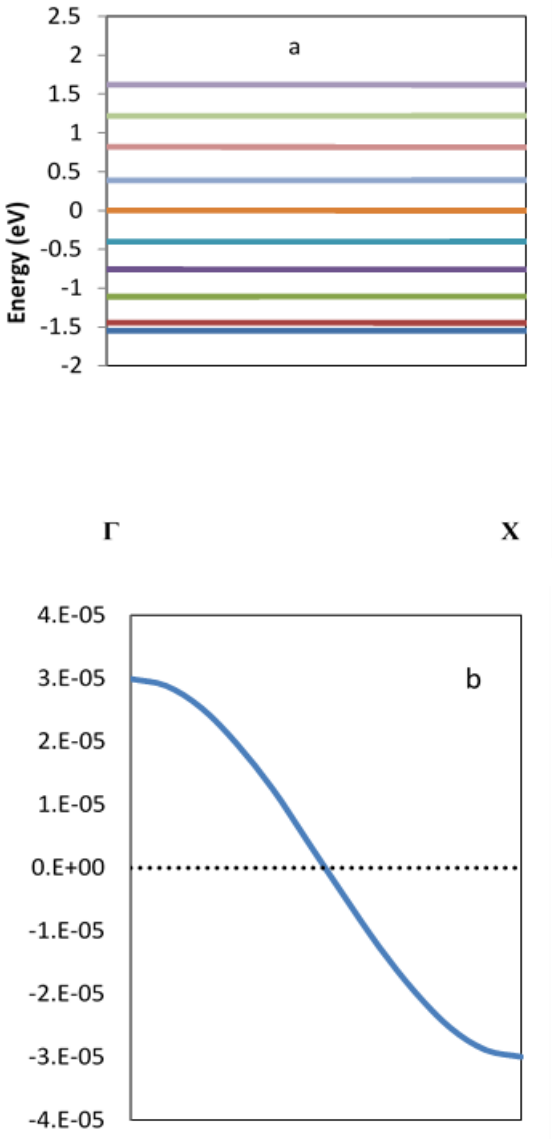

Figure 6. a) Calculated band structure of $M20^{+}$. b) Valance band. The band structures are plotted along the high symmetry path: Γ (0, 0, 0) → X (0.5, 0, 0). The Fermi level is shifted to 0 eV.

3.2 Electron transport

The predicted transmission functions are evaluated in order to investigate the electronic transport properties in the AGNRs. The Fig 7 illustrates the transmission probability (Tr) at zero applied voltage versus the energy of the five ribbons. The plots show the semi-metal transition of junctions. For the 5-AGNRs, the two peaks present at the left and right sides of the Fermi level as the bias are zero. Undoubtedly, they respectively refer to the highest occupied molecular orbital (HOMO) and the lowest unoccupied molecular orbital (LUMO) of the systems. The finite gap in the transmission spectra means electron can transmit beyond a threshold bias voltage, which this feature may be utilized in fabrication of Nano-electronic devices. It is known that a transmission function against energy is quantized in an intrinsic AGNR with infinite length. In the G-AGNR-G system which is connect to semi-infinite graphene electrodes, the quantization is collapsed. Likewise, the step-like behavior of the spectrum is related with the available conductance channels due to bands.

The transmission of 5-AGNRs show semiconductor characteristic with the energy windows as listed in table 2. The energy window of transmission enlarges with nanoribbon length increase. Our results show that, the presence of positive charge in $M20^{+}$ strip tends to the appearance of a more wider gap in the conductance spectrum than the neutral system M20, Fig 8, because of it released an electron and deficient density of states near Fermi level. It indicates that by controlling the length or charge state, the conductance of the formed junction could be tuned to be either small or large. The transmission at a given electron energy is equal to the electron transmission probability times the

number of channels, but in case of perfect molecule, the transmission without scattering (i.e. transmission probability equal to 1) is simply equal to the number of channels. The magnitude of the change in transmission represents the sub-band degeneracy of the band structure and each contributes one channel for transmission.

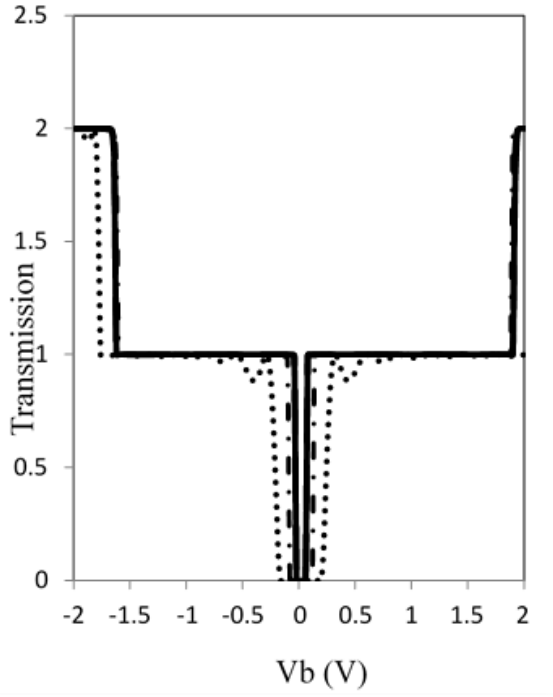

Figure 7. The transmission Tr in unit (G_o) of M4 (line), M12 (dash), M20 (dash dots) and M28 (dot).

Table 2. Transmission window T_w and threshold voltage V_{th}.

Property (V)	T_w	V_{th}
M4	-0.04 – 0.08	0.10
M12	-0.06 – 0.10	0.10
M20	-0.14 – 0.18	0.20
M20+	-0.42 – 0.46	0.40
M28	-0.28 – 0.32	0.00

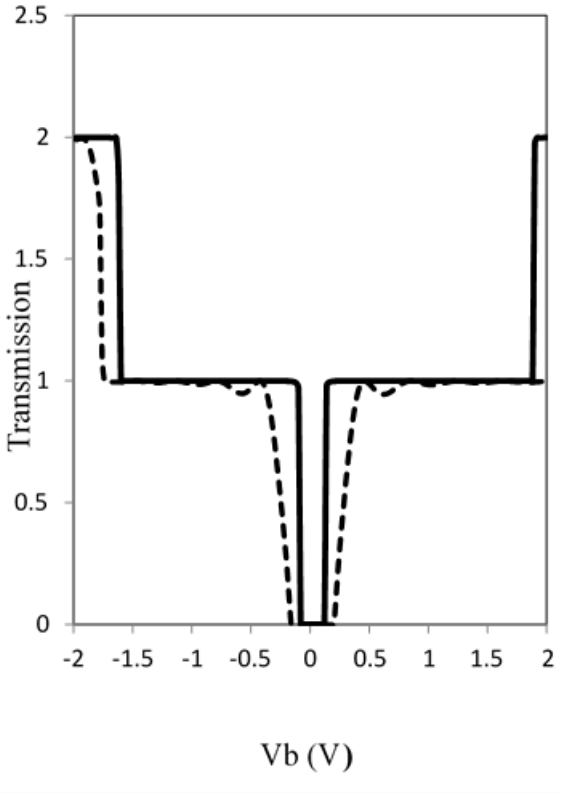

Figure 8. The transmission Tr in unit (G_o) of M20 (line) and $M20^+$ (dotted).

Symmetric AGNRs behave as conventional semiconductors with the presence of a conductance gap around the Fermi level, and exhibit unexpected threshold current-voltage dependence with very small currents. The Current-Voltage (I-V) characteristics for the structures, which is compared between each other, were studied by applying the voltage between 0.0V and 1.0V as shown in Fig 8. From the curves obtained it is observed that the graphene nanoribbons exhibit an interesting behavior. As shown clearly, the current in each device begins to flow at a different bias voltage, and the threshold of the junctions is sensitive to the length and charge state of the embedded 5-AGNR. This changed threshold voltage implies that the existence of structural effects on the

transport energy gap. Reflecting the distributions of the transmission functions, the electron transport property is semiconductor like conductivity. With the bias increasing, both of HOMO and LUMO extend gradually to the Fermi level and overlap at threshold bias voltage. Unambiguously, it is the overlap between HOMO and LUMO that forms the first transport channel in the perfect AGNR. Thus, the current starts to flow at this point. As a result, the current increases with the increase of the applied voltage as shown. With the increase of bias larger the threshold, the I-V curve presents a parabolic growth trend. The dependence of the Dirac electron tunneling current on the source voltage for different 5-AGNR lengths is depicted in Fig 9. In addition, the 5-AGNRs band gaps is inversely proportional to the strips length. As the AGNR length increases, its band-gap decreases, hence less electron densities are allowed at Fermi energy. As a result, the Dirac electron tunneling current decreases. In the case of nanoribbon M28, for low bias voltages current flow is negligible. As the voltage bias is increased, at a particular voltage(cut-in voltage), conduction starts and a linear curve is obtained there on.

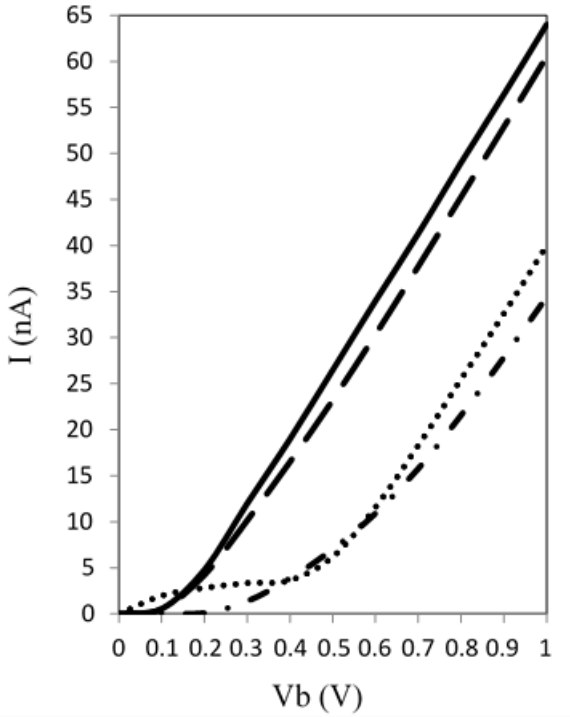

Fig 9: The current-voltage characteristic of M4 (line), M12 (dash), M20 (dash dot) and M28 (dot).

As shown in Fig 10, $M20^{+}$ systems does not exhibit a significant current until 0.4 V, larger than M20 threshold 0.2 V. Afterwards, at ~0.6 intersects the current curve of M20 and exhibit larger current than the uncharged system. The explanation of this large bias threshold is the charge state, where charge doping by interfacial charge transfer shifts the Fermi-level toward the valance band. A downward shift of the Fermi-level (p-type charge-doping) decreases the electron densities at Fermi energy. On the other hand, the valance band of $M20^{+}$ crosses the Fermi level as shown in Fig 6. According to this it is presence a nearly flat half occupied metallic band. Thus, the drain current beyond threshold bias will be larger than that of uncharged M20 system.

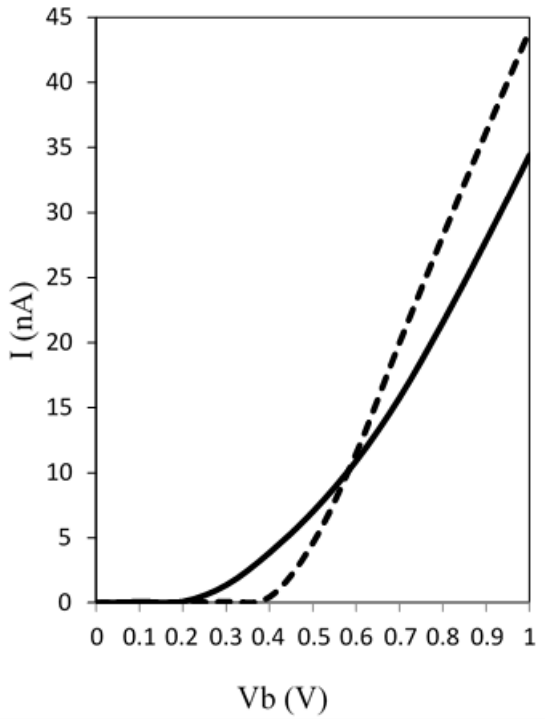

Fig 10: The current-voltage characteristic of M20 (line) and $M20^{+}$ (dot).

4. CONCLUSIONS:

The band structures and transport properties of short ultrathin 5-AGNRs with diff erent lengths have been systematically investigated, using a nonequilibrium Green's function formalism in combination with density functional tight binding method. The electronic behavior is modified by changing the length, since the nanoribbons present a direct band gap at the gamma point; nevertheless, the band gap is opened with the reduction of strip length. However, in 5-AGNRs, positive charge-doping introduces a flat half-filled band, and induces a semi-metallic electronic structure by lowering the Fermi level. It has shown that the 5-AGNR devices can exhibit remarkable semiconductor current behavior in spite of the presence of the transmission gap.

5. ACKNOWLEDGMENT:

The author is grateful to the anonymous referees for their suggestions.

6. REFERENCES

[1] Yang, L., Park, C., Son, Y., Cohen, M. & Louie, S., "Quasiparticle Energies and Band Gaps in Graphene Nanoribbons". Phys. Rev. Lett., Vol. 99, 186801, 2007.

[2] Han, M. Y., Ozyilmaz, B., Zhang, Y. B., & Kim, P. "Energy Band-Gap Engineering of Graphene Nanoribbons", Phys. Rev. Lett., Vol. 98, 206805, 2007.

[3] Wang, X., Ouyang, Y., Li, X., Wang, H., Guo, J. & Dai, H., "Room-Temperature All-Semiconducting Sub-10-nm Graphene Nanoribbon Field-Effect Transistors", Phys. Rev. Lett., Vol. 100, 206803, 2008.

[4] Martins, T. B., da Silva, A. J. R., Miwa, R. H. & Fazzio, A. , "σ- and π-Defects at Graphene Nanoribbon Edges: Building Spin Filters", Nano Lett., Vol. 8, pp. 2293-2298, 2008.

[5] Brey, L. & Fertig, H. A. , " Edge states and the quantized Hall effect in graphene", Phys. Rev. Lett. B, Vol. 73, 235911, 2006.

[6] Wakabayashi, K., Fujita, M., Ajiki, H. & Sigrist, M. , "Electronic and magnetic properties of nanographite ribbons", Phys. Rev. B, Vol. 59, 8271, 1999.

[7] Ezawa, M., "Peculiar width dependence of the electronic

properties of carbon nanoribbons", Phys. Rev. B, Vol. 73, 045432, 2006.

[8] Barone, V., Hod, O. & Scuseria, G. E., "Electronic Structure and Stability of Semiconducting Graphene Nanoribbons", Nano Lett., Vol. 6, 2748-2754, 2006.

[9] Yazyev, O. V., "A Guide to the Design of Electronic Properties of Graphene Nanoribbons", Acc. Chem. Res., Vol. 46, pp. 2319-2328, 2013.

[10] Zhao, P. & Guo, J., "Modeling edge effects in graphene nanoribbon field-effect transistors with real and mode space methods", J. Appl. Phys., Vol. 105, 034503, 2009.

[11] Chen, Y. C., Cao, T., Chen, C., Pedramrazi, Z., Haberer, D., de Oteyza, D. G., Felix, R., Fischer, F. R., Louie, S. G. & Crommie, M. F., "Molecular bandgap engineering of bottom-up synthesized graphene nanoribbon heterojunctions", Nature Nanotechnology, Vol. 10, pp. 156-161, 2015.

[12] Narita, A., Verzhbitskiy, I. A., Frederickx, W., Mali, K. S., Jensen, S. A., Hansen, M. R., Bonn, M., De Feyter, S., Casiraghi, C., Feng, X. & Mu¨llen, K., "Bottom-Up Synthesis of Liquid-Phase-Processable Graphene Nanoribbons with Near-Infrared Absorption", ACS Nano, Vol. 8, 11622, 2014.

[13] Yang, X., Dou, X., Rouhanipour, A., Zhi, L., Rader, H. J. & Mullen, K., "Two-Dimensional Graphene Nanoribbons. J. Am. Chem. Soc., Vol. 130, pp. 4216-4217, 2008.

[14] Talirz, L., So¨de, H., Dumslaff, T., Wang, S., Sanchez-Valencia, J. R., Liu, J., Shinde, P., Pignedoli, C., Liang, L., Meunier, V., Plumb, N. C., Shi, M., Feng, X., Narita, A., Mu¨llen, K., Fasel, R. & Ruffieux, P., "On-Surface Synthesis and haracterization of 9- Atom Wide Armchair Graphene Nanoribbons", ACS Nano, Vol. 11, pp. 1380-1388, 2017.

[15] Chen, Z., Wang, H. I., Teyssandier, J., Mali, K. S., Dumslaff, T., Ivanov, I., Zhang, W., Ruffieux, P., Fasel, R., Ra¨der, H. J., Turchinovich, D., De Feyter. S., Feng, X., Kla¨ui, M., Narita, A., Bonn, M. & Mu¨llen, K. J., "Chemical vapor deposition synthesis and terahertz photoconductivity of low-bandgap N = 9 armchair graphene nanoribbons", J. Am. Chem. Soc., Vol. 139, pp. 3635-3641, 2017.

[16] Moreno, C., Vilas-Varela M. M., Kretz, B., Garcia-Lekue, A., Costache, M. V., Paradinas, M., Panighel, M., Ceballos, G., Sergio, O., Valenzuela, S. O., Peña, D. & Mugarza, A. "Bottom-up synthesis of multifunctional nanoporous grapheme", Science, Vol. 360, pp. 199-203, 2018.

[17] Simonov, K.A., Generalov, A. V., Vinogradov, A. S., Svirskiy, G. I., Cafolla, A. A., McGuinness, C., Taketsugu, T., Lyalin, A., Mårtensson, N. & Preobrajenski, A. B., "Synthesis of armchair 71rapheme nanoribbons from the 10,10′-dibromo-9,9′-bianthracene molecules on Ag(111): the role of organometallic intermediates", Scientific Reports, Vol. 8, 3506, 2018.

[18] Merino-Diez, N., Garcia-Lekue, A., Eduard Carbonell-Sanroma, E., Li, J., Corso, M., Colazzo, L., Sedona, F., Sanchez-Portal, D., Jose I. Pascual, J. I. & de Oteyza, D. G., "Width-Dependent Band Gap in Armchair

Graphene Nanoribbons Reveals Fermi Level Pinning on Au(111)", ACS Nano, Vol. 11, pp. 11661−11668, 2017.

[19] Ma, C., Liang, L., Xiao, Z., Puretzky, A. A., Hong, K., Lu, W., Meunier, V., Bernholc, J. & Li, A. P., "Seamless staircase electrical contact to semiconducting graphene nanoribbon", Nano Lett., Vol. 17, pp. 6241, 2017.

[20] So¨de, H., Talirz, L., Gro¨ning, O., Pignedoli, C. A., Berger, R., Feng, X., Mu¨llen, K., Fasel, R. & Ruffieux, P., "Electronic band dispersion of graphene nanoribbons via Fourier-transformed scanning tunneling spectroscopy", Phys. Rev. B, Vol. 91, 45429, 2015.

[21] Wu, Y. & Childs, P. A., "Conductance of Graphene Nanoribbon Junctions and the Tight Binding Model", Nanoscale Res. Lett., Vol. 6, 62, 2011.

[22] Liu-Jun, Z. & Tong-Sheng, X., "The complex band structure for armchair graphene nanoribbons", Chin. Phys. B, Vol. 19, 117105, 2010.

[23] Jain, M., Chelikowsky, J. R. & Louie, S. G., "Reliability of Hybrid Functionals in Predicting Band Gaps", Phys. Rev. Lett., Vol. 107, 216806, 2011.

[24] Ma, F., Guo, Z., Xu, K. & Chu, P. K., "First-principle study of energy band structure of armchair graphene nanoribbons", Solid State Communications, Vol. 152. 1089, 2012.

[25] Novoselov, K. S., Geim, A. K., Morozov, S. V., Jiang, D., Katsnelson, M. I., Grigorieva, I. V., Dubonos, S. V. & Firsov, A. A., "Two-dimensional gas of massless Dirac fermions in graphene", Nature (London), Vol. 438, pp. 197-200, 2005.

[26] Reimers, J. R., Gemma C. Solomon, G. C., Gagliardi, A., Ante Bilic, A., Hush, N. S., Frauenheim, T., Di Carlo, A. & Alessandro Pecchia, A., "The Green's Function Density Functional Tight-Binding (gDFTB) Method for Molecular Electronic Conduction", J. Phys. Chem. A, Vol. 111, pp. 5692-5702, 2007.

[27] Kimouche, A., Ervasti, M. M., Drost, R., Halonen, S., Harju, A., Joensuu, P. M., Sainio, J. & Liljeroth, P., "Ultra-narrow metallic armchair grapheme nanoribbons", Nature Communi-cations, Vol. 6, 10177, 2015.

[28] Zhang, X. H., Li, X. F. & Qiu, Q., "Isolated pentagons induced enhancement of conductance in ultra-narrow armchair graphene nanoribbon junctions", J. Appl. Phys., Vol. 120, 164303, 2016.

[29] Elias, D. C., Gorbachev, R. V., Mayorov, A. S., Morozov, S. V., Zhukov, A. A., Blake, P., Ponomarenko, L. A., Grigorieva, I. V., Novoselov, K. S., Guinea, F. &. Geim, A. K., "Dirac cones reshaped by interaction effects in suspended grapheme", Nat. Phys., Vol. 7, 701, 2011.

[30] Li, G., Luican, A. & Andrei, E. Y., "Scanning Tunneling Spectroscopy of Graphene on Graphite", Phys. Rev. Lett., Vol. 102, 176804, 2009.

[31] Hwang, C., Siegel, D. A., Mo, S. K., Regan, W., Ismach, A., Zhang, Y., Zettl, A. & Lanzara, A., "Fermi velocity engineering in graphene by substrate modification", Scientific Reports, Vol. 2, 590, 2012.